Bubbling transition

Shankar C. Venkataramani,[1,*] Brian R. Hunt,[2] and Edward Ott[1,3]
[1]*Department of Physics and Institute for Plasma Research, University of Maryland, College Park, Maryland 20742*
[2]*Institute for Physical Science and Technology, University of Maryland, College Park, Maryland 20742*
[3]*Department of Electrical Engineering and Institute for Systems Research, University of Maryland, College Park, Maryland 20742*
(Received 5 February 1996; revised manuscript received 25 April 1996)

Recently, physically important examples of dynamical systems that have a chaotic attractor embedded in an invariant submanifold have been pointed out, and the unusual dynamical consequences of this situation have been studied. As a parameter ϵ of the system is increased, a periodic orbit embedded in the attractor on the invariant manifold can become unstable for perturbations transverse to the invariant manifold. This bifurcation is called the *bubbling transition*, and it can lead to the occurrence of a recently discovered, new kind of basin of attraction, called a *riddled basin*. In this paper we study the effects of noise and asymmetry on the bubbling transition. We find that, in the presence of noise or asymmetry, the attractor is replaced either by a chaotic transient or an intermittently bursting time evolution, and we derive scaling relations, valid near the bubbling transition, for the characteristic time (i.e., the average chaotic transient lifetime or the average interburst time interval) as a function of the strength of the asymmetry and the variance of the additive noise. We also present numerical evidence for the predicted scalings. [S1063-651X(96)12508-3]

PACS number(s): 05.45.+b

I. INTRODUCTION

Many chaotic dynamical systems of physical interest possess symmetries. These systems have invariant manifolds embedded in their phase space, since any initial state that has the same symmetry as the entire system evolves to other states that also respect the symmetry of the system. The set of such symmetric initial states then forms a manifold that is invariant under the system dynamics. These invariant manifolds can also have the property that the dynamics restricted to the manifold is chaotic, i.e., symmetric initial states can be attracted to a chaotic set in the invariant manifold. This situation occurs naturally in the context of systems with spatial symmetry or in the synchronization of chaotic oscillators [1,2].

For example, in the case of synchronization of identical chaotic oscillators, the set of all synchronized states is an invariant manifold. Figure 1 is a schematic illustration of two identical coupled chaotic oscillators.The vectors $\overline{u}$ and $\overline{v}$ represent the states of the two oscillators. Consider the situation where the dynamics of each oscillator without the coupling is chaotic and has a chaotic attractor. In the figure, the oscillators are coupled diffusively, i.e., the coupling is given by the difference between the states of the two oscillators. Consequently, if the two oscillators are synchronized at some instant of time, the coupling between them is zero. If the oscillators are identical, they will remain synchronized for all later times in the absence of noise or external perturbations, implying that the set of all synchronized states is an invariant manifold, the *synchronization manifold*.

On the synchronization manifold, the dynamics of the system are the same as that of a single free-running oscillator. Therefore, the coupled system has a chaotic attractor for the dynamics restricted to the synchronization manifold. This situation is illustrated schematically in Fig. 2. (The attractor embedded in the manifold will be denoted by A.)

As another example consider the case of time-dependent Rayleigh-Bénard convection in a cell with a symmetry plane about the middle of the cell. This is illustrated in Fig. 3 where the symmetry plane of the cell is shown as a dashed line. In principle, if an initial condition is set up with the same symmetry as the cell, it will retain that symmetry for all time. The full dynamics, however, allows asymmetric motions in addition to the symmetric motions. The set of all symmetric states thus represents an invariant manifold in the full state space of the dynamical system (analogous to the synchronization manifold for the system in Fig. 1).

Recent work [1–7] has investigated the consequences of an invariant manifold embedded in the phase space such that the dimension of the invariant manifold is less than the dimension of the phase space and the dynamics restricted to the invariant manifold has a chaotic attractor. A question of considerable interest is the stability of the attractor in the invariant manifold, i.e., the conditions under which the attractor A on the invariant manifold is also an attractor for the

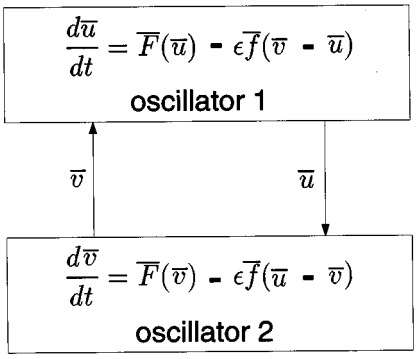

FIG. 1. Coupled identical chaotic oscillators. The coupling is the same in both directions.

*Electronic address: cat@fractal.umd.edu

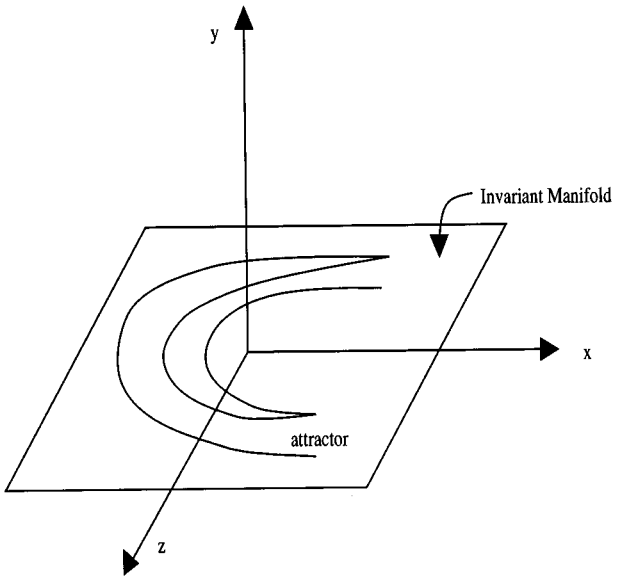

FIG. 2. A schematic of an invariant manifold with an embedded attractor. For initial conditions in the invariant manifold, the subsequent orbit remains in the manifold and eventually ends up on the attractor.

dynamics in the entire phase space. For example, if this is the case in the system of coupled oscillators, the oscillators will eventually synchronize. If this is the case for the Rayleigh-Bénard example (Fig. 3), an initial spatially asymmetric state can evolve to a spatially symmetric state. A natural question is what happens to this attractor under perturbations due to noise. Another is what happens in the presence of small spatial asymmetry in a case like the Rayleigh-Bénard example, or in the presence of a small mismatch between the two oscillators. These questions are of experimental interest in determining the conditions under which the two oscillators will synchronize and then stay locked or whether the Rayleigh-Bènard system evolves toward the symmetric state and stays there.

Ashwin *et al.* [2] consider the situation where there exists a parameter that affects the dynamics transverse to the invariant manifold but does not affect the dynamics on the invariant manifold. They call such a parameter a *normal parameter*. In the case of coupled oscillators considered above, ϵ, the strength of the coupling between the oscillators is a normal parameter. In Ref. [2] they consider the situation where ϵ is a normal parameter and there exists a critical value ϵ_b of ϵ, such that for $\epsilon<\epsilon_b$ all invariant sets in the attractor A are stable with respect to perturbations in a direction transverse to the invariant manifold, and as ϵ is increased through ϵ_b an invariant set embedded in the attractor A first becomes unstable to perturbations in a transverse direction. In this case, for $\epsilon<\epsilon_b$, all orbits that start with initial conditions sufficiently close to A asymptotically approach A [8].

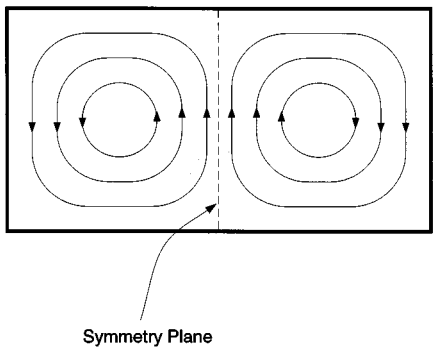

FIG. 3. A symmetric Rayleigh-Bénard cell with symmetric convection rolls.

When ϵ slightly exceeds ϵ_b, most initial conditions close to A remain close to A and are attracted to A. However, as a consequence of the invariant set embedded in A that is repelling in the transverse direction, there is also a small set of points in any neighborhood of A that move far from the invariant manifold containing A. The transition at $\epsilon=\epsilon_b$ is called the *bubbling transition* [1].

If the global dynamics of the system are such that these repelled orbits are attracted to a set off the invariant manifold, then the basin of attraction of A is *riddled* [6] and A is no longer a topological attractor. It is a *Milnor attractor*; i.e., it attracts a set of inital conditions with positive Lebesgue measure. However, there is no neighborhood of the attractor A for which *all* initial conditions are attracted by A. The basin of A is ''riddled'' by pieces of the basin(s) of the attracting set(s) off the invariant manifold in the sense that a sphere of arbitrarily small radius ϵ centered about any point in the basin of A has a positive fraction of its volume occupied by points in the basin(s) of the other attractor(s). This has the disturbing consequence that, if one does an experiment setting an initial condition and observing that it goes to the riddled basin attractor, repeating this may lead to a different attractor with a finite probability even if the experimental error in setting the initial condition can be made arbitrarily small. The unusual properties of riddled basins have received much recent attention [5–7].

On the other hand, if the global dynamics of the system are bounded and there exist no attractors other than A, then an orbit repelled from A will eventually return to the vicinity of the invariant manifold, possibly after a transient phase in which the orbit makes several excursions (bursts) away from the invaraint manifold. In this case, almost all orbits eventually end up on the attractor A.

Dynamical systems with invariant manifolds are not generic. For example, in cases where the invariant manifold is a consequence of a symmetry in the system, a small asymmetry or additive noise, both of which will be present in real systems, will destroy the invariant manifold [9]. Thus, it is of interest to study the effect of noise and small asymmetry on the dynamics of systems that would possess invariant manifolds if the symmetry was exact and there was no additive noise. In this paper, we study the effects of a small asymmetry [10] and additive noise on the bubbling transition at $\epsilon=\epsilon_b$.

We consider a dynamical system with a parameter q that controls the amplitude of the asymmetry or the noise in the system. When $q=0$, the system has an invariant manifold. As discussed above, when $\epsilon>\epsilon_b$, there are two cases of interest:

(i) There are other attractors not on the $q=0$ invariant manifold and the attractor on the invariant manifold has a riddled basin;

(ii) There are no attractors other than the one in the invariant manifold.

In case (i) as ϵ is increased through ϵ_b the basin of the attractor in the invariant manifold becomes riddled when $q=0$. We find that the presence of small noise or asymmetry has the following effects in the two cases. In case (i) an orbit can be attracted to the neighborhood of the attractor that would exist on the invariant manifold in the absence of noise or asymmetry. The orbit then behaves chaotically in this neighborhood in a manner similar to the noiseless symmetric case. This, however, does not persist forever, and, after some time, the orbit will leave this neighborhood. The quantity of interest in this case is the average time the orbit spends near the ''ghost'' of the attractor for the noiseless symmetric case. In case (ii) an orbit near the ghost attractor (formerly on the invariant manifold) again leaves its vicinity and goes far away. In this case, however, there is no other attractor to capture this orbit. The orbit thus eventually returns to the ghost attractor and stays in its vicinity before again bursting away. In both cases, the mechanism by which the orbit leaves the ghost attractor is the same, and the quantity of interest is the average time spent there. Thus one of our goals in this paper is to uncover the scaling of this average time as a function of the asymmetry amplitude and the noise amplitude when these amplitudes are small and ϵ is near ϵ_b.

Our results highlight the issue of the observability of riddled basins in experiments. Strictly speaking, the riddled basin attractor on the invariant manifold does not exist when noise and asymmetry are present. However, experimentally this may not matter, provided the transient lifetime on the ghost attractor is much larger than the duration of the experiment. (This was apparently the case for the experiment in Ref. [11].) In order to quantitatively assess if this is the case, it is crucial to have an estimate of the transient lifetime.

Our results are also relevant in the problem of synchronization of chaotic oscillators. If there is no noise in the system and the oscillators are identical, the synchronized state is an invariant manifold in the phase space of the coupled system. If this manifold is attracting on average (i.e., all the Lyapunov exponents for perturbations transverse to the invariant manifold are negative), the coupled system will eventually settle in the synchronized state. However, as observed in the experiments [12,13], a small noise in the system or a small mismatch between the oscillators will cause the system to burst away from the synchronized state even if the synchronized state is attracting on average. Our results give us a quantitative estimate (for the case of a system near the bubbling transition) of the average interburst interval and the distribution of interburst intervals. This is crucial in order to estimate the time that the coupled oscillators will stay in phase.

This paper is organized as follows. In Sec. II we introduce a two-dimensional (2D) map that we use to study the effects of noise and asymmetry on the bubbling transition. In Sec. III we state our results for the effects of noise and asymmetry on the bubbling transition. In Sec. IV we give a general formula for the escape time. In Sec. V we derive our results for the effect of asymmetry. In Sec. VI we derive our results for the effect of additive noise. In Sec. VII we translate the results derived for the riddled basin case in Secs. II–VI to the case where there is only one attractor in the system (i.e., the case of intermittent bursting). Section VIII considers the case of synchronized oscillators in which the coupling is not symmetric. In this case, the invariant manifold is not due to a symmetry and different scaling results are obtained.

II. THE MODEL

The universality of the phenomena addressed in this paper implies that very general results may be extracted from simple models that incorporate the essential features responsible for these phenomena. In this spirit we introduce the following two dimensional map:

$$x_{n+1}=2x_n \bmod 1,$$

$$y_{n+1}=\{1+\epsilon-r[1-\cos(2\pi x_n)]\}y_n+y_n^3 + q[\delta_1\sin(2\pi x_n+\gamma)+\delta_2\nu_n], \tag{1}$$

where ν_n are zero mean, independent, identically distributed random variables chosen at each iterate n of the map and have a variance $E[\nu_n^2]=1$. The case $q=0$ corresponds to the symmetric noiseless case. In particular, note that when $q=0$, the system has the symmetry $y\to -y$. The symmetry $y\to -y$ in (1) models the spatial symmetry in a situation like Fig. 3. It is, as discussed subsequently, also appropriate to coupled oscillators when the coupling is symmetric (as in Fig. 1). As a consequence of the $y\to -y$ symmetry, the manifold $y=0$ is invariant under the action of the map (1) when $q=0$. The dynamics on this invariant manifold are generated by the $2x \bmod 1$ map and are independent of ϵ and r. Therefore, the parameters ϵ and r are normal parameters for the system in (1) with $q=0$.

In subsequent sections of this paper we shall separately consider the effect of asymmetry in the absence of noise, which corresponds to

$$q\neq 0, \quad \delta_1=1, \quad \delta_2=0,$$

and the effect of noise in the absence of asymmetry, which corresponds to

$$q\neq 0, \quad \delta_1=0, \quad \delta_2=1.$$

With this convention, the parameter q controls the strength of the asymmetry in the first case, while in the second case it controls the strength of the noise.

Note that in (1) the noise occurs only in the y component of the map. In a realistic situation this would not be expected, and a more isotropic noise model is appropriate. To achieve this, one could replace the equation for x_n in (1) by

$$x_{n+1}=(2x_n+\overline{q}\,\overline{\delta}_2\,\overline{\nu}_n) \bmod 1, \tag{2}$$

where $\overline{\nu}_n$ is randomly chosen at each iterate with variance $E[\overline{\nu}_n^2]=1$, $\overline{q}$ characterizes the strength of the noise in the x direction, and $\overline{q}\sim q$. We show in Sec. VI B, however, that in the parameter regime we consider such x noise has no effect on the scaling results we obtain. Thus, for simplicity,

we shall henceforth take $\overline{q}=0$ (except in Sec. VI B). In the remainder of this section we consider the symmetric noiseless case $q=0$.

The choice of the sign of the nonlinear term, $+y_n^3$ in (1), leads to orbits that asymptote to $y=\pm\infty$. In what follows we regard $|y|=\infty$ as an attractor. As shown below, when $q=0$ and $\epsilon_b<\epsilon$, the basin of the $y=0$ attractor is riddled by the basin of the $|y|=\infty$ attractor. The case of a confining nonlinearity, $-y_n^3$, is considered in Sec. VII.

For definiteness, throughout most of this paper, we consider the bubbling transition for the case of riddled basins. We emphasize that, as discussed in Sec. I, all our results carry over directly to the case when the global dynamics is such that the only attractor is on the invariant manifold ($y=0$) and asymmetry or noise then induces intermittent bursting (see Sec. VII).

Consider the case $q=0$ (no asymmetry or noise). If we are close to the invariant manifold $y=0$, we can neglect the y_n^3 nonlinearity in (1). With this approximation, an orbit is given by

$$x_n=2^n x_0,$$

$$y_n=\lambda(2^{n-1}x_0)\lambda(2^{n-2}x_0)\cdots\lambda(x_0)y_0, \tag{3}$$

where

$$\lambda(x)=\{1+\epsilon-r[1-\cos(2\pi x)]\}, \tag{4}$$

and we have used the notation $2^n x$ to denote $2^n x \bmod 1$. If $\epsilon<0$, $|\lambda(x)|\leq 1-|\epsilon|$ for all $x\in[0,1)$. Therefore,

$$\lim_{n\to\infty}|\lambda(2^{n-1}x_0)\lambda(2^{n-2}x_0)\cdots\lambda(x_0)|\leq\lim_{n\to\infty}(1-|\epsilon|)^n=0. \tag{5}$$

This implies that for a sufficiently small y_0, an orbit starting at (x_0,y_0) is attracted to the invariant manifold $y=0$ for all x_0. Therefore, the set $y=0$ is an attractor for the dynamical system in (1) when $\epsilon<0$.

Again considering the noiseless symmetric case ($q=0$), if $\epsilon>0$, then $\lambda(0)=1+\epsilon>1$. Therefore, an orbit with initial conditions $(0,y_0\neq 0)$ is repelled by the fixed point at (0,0). Since the y_n^3 nonlinearity is also repelling (i.e., it does not cause the orbit to be bounded), an orbit starting at $(0,y_0)$ is repelled to $y=\pm\infty$. Thus, there are points arbitrarily close to the invariant manifold that are repelled to $\pm\infty$. This implies that the invariant manifold is no longer a topological attractor. However, a typical orbit of the $2x \bmod 1$ map is distributed uniformly in $[0,1]$, and for $0<\epsilon$ and ϵ not too large, the invariant manifold ($y=0$) is still attracting on average, i.e.,

$$\lim_{n\to\infty}\log|\lambda(2^{n-1}x_0)\lambda(2^{n-2}x_0)\cdots\lambda(x_0)|^{1/n}$$

$$=\int\log|\lambda(x)|dx<0, \tag{6}$$

for a typical initial $x_0\in[0,1)$. Therefore, for a typical $x_0\in[0,1)$ and sufficiently small y_0, we have $y_n\to 0$. Here by typical we mean that the set of x_0 for which (6) is not true has zero Lebesgue measure (e.g., the preimages of $x=0$ are part of the nontypical set). The invariant manifold is therefore a Milnor attractor and a bubbling transition occurs at $\epsilon=\epsilon_b=0$. In this case the basin of the attractor on $y=0$ is riddled by the basin of the attractor at $|y|=\infty$. That is, every ball centered on an initial condition (x_0,y_0) which generates an orbit going to the $y=0$ attractor has pieces of the $|y|=\infty$ basin within it, and this is true no matter how small the radius of the ball is. Figure 4 shows a numerically generated picture of the basin of the $y=0$ attractor basin (blank) and the $|y|=\infty$ basin (black) for the system in (1) with $q=0$, $\epsilon=0.2$, and $r=0.8$.

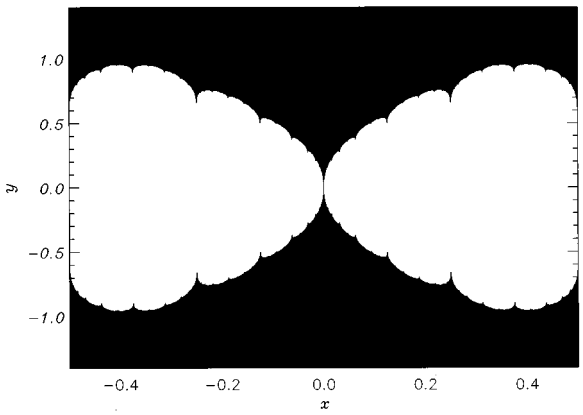

FIG. 4. The basin of attraction of the $|y|=\infty$ attractor for the system in (1) with $q=0$. We have $\epsilon=0.2$. The figure is generated with a resolution of approximately 1/5000 in the x direction so that structures whose widths are narrower than 1/5000 do not show up. Although the white basin looks solid, it is actually riddled by thin ''tongues'' of the black basin that emerge from the preimages of $x=0$ on the $y=0$ line.

As discussed in [1,2] the bubbling transition occurs at a parameter value $\epsilon=\epsilon_b$ if as ϵ is increased through ϵ_b an invariant set embedded in the chaotic attractor first becomes unstable to perturbations transverse to the invariant manifold. For our example, Eq. (1), the first invariant set to become transversely unstable is the period one orbit, $x=0$, $y=0$ and this occurs at $\epsilon=0$. Thus the bubbling transition is mediated by this particular orbit with $\epsilon_b=0$. More generally, the authors of [14] have shown that, except in exceptional situations, the invariant set whose stability mediates the transition is a periodic orbit, and the orbit is usually of low period [15]. It can be shown that the results are independent of the period of the orbit that mediates the transition, so that no generality is lost by taking the period to be one in our numerical experiments or in our subsequent analysis.

Because of the y_n^3 nonlinearity, the system in (1) has the property that for any given ϵ, q, and $\delta>0$, there exists a smallest threshold y_{max} such that

$$\frac{y_{n+1}}{y_n}>(1+\delta), \tag{7}$$

independent of x_n if $|y_n|>y_{max}$. Therefore, every orbit that ends up outside the band $|y|\leq y_{max}$ is attracted to $y=\pm\infty$. As we shall see later, if $q\neq 0$ and $\epsilon>0$, there is no attractor near the invariant manifold and all orbits are attracted to $\pm\infty$. We define the escape time as the average time that a typical orbit takes to leave a neighborhood of the invariant

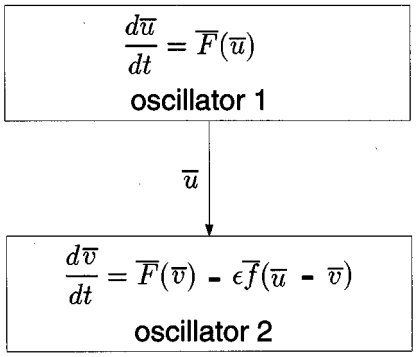

FIG. 5. Coupled identical chaotic oscillators. The coupling is one way.

manifold and never return. For our simulations we use the neighborhood $|y|<y_{max}$ to calculate the escape times (defined more precisely below).

To close this section we comment on the relevance to experiments of our hypothesis that there is a symmetry with respect to the invariant manifold. Various physical cases where a symmetry induces an invariant manifold can be envisioned. For example, Fig. 3 depicts a situation of Rayleigh-Bénard convection in a spatially symmetric container, and Eqs. (1) are expected to be a valid model of the qualitative behavior of such a system if it undergoes a bubbling transition. A second example, depicted in Fig. 1, is the system in which occurs symmetrically coupled identical chaotic oscillators. In the case with two oscillators (see Fig. 1) we have

$$\frac{d\overline{u}}{dt}=\overline{F(\overline{u})}+\epsilon\overline{f(\overline{u}-\overline{v})},$$

$$\frac{d\overline{v}}{dt}=\overline{F(\overline{v})}+\epsilon\overline{f(\overline{v}-\overline{u})},$$

where ϵ is a coupling strength and $\overline{f(0)}=0$. This system is symmetric to the interchange of $\overline{u}$ and $\overline{v}$ and we again expect Eq. (1) to be a good model of what happens when asymmetry and/or noise is introduced. Here x and y of (1) can be identified with $(\overline{u}+\overline{v})/2$ and $\overline{u}-\overline{v}$, and the invariant manifold is the synchronized state $\overline{u}=\overline{v}$.

Another, quite different situation occurs when the two oscillators are not coupled symmetrically (see Fig. 5). For example, Gauthier and Bienfang [12] experimentally investigate a case of one-way coupling of two oscillators,

$$\frac{d\overline{u}}{dt}=\overline{F(\overline{u})},$$

$$\frac{d\overline{v}}{dt}=\overline{F(\overline{v})}+\epsilon\overline{f(\overline{v}-\overline{u})}.$$

Again, the synchronized state $\overline{u}=\overline{v}$ is an invariant manifold. This system, however, is asymmetric in the sense that it is *not* invariant to interchange of the variable $\overline{u}$ and $\overline{v}$. As a consequence, we do not expect Eqs. (1) to be the proper generic model for this system. In particular, the lowest order nonlinearity to be expected is y^2 rather than y^3.

Our use of y^3 in (1) arises from the assumption that the invariant manifold is accompanied by a symmetry, which requires that the model be invariant under the transformation $y\rightarrow -y$. This invariance rules out a y^2 nonlinearity and the lowest order nonlinearity that is admissible is y^3. For the case of one-way coupling, due to the absence of the $y\rightarrow -y$ type symmetry, the lowest order nonlinearity will be y^2 generically.

In most of this paper (Secs. II–VII), we only consider the case of symmetry about the invariant manifold, for which Eqs. (1) are a valid model. The case where the y^3 nonlinearity is replaced by a y^2 nonlinearity (appropriate, for example, to synchronization by one-way coupling) yields results that differ in essential ways from the y^3 nonlinearity case, and is discussed in Sec. VIII.

III. RESULTS

Let X denote the invariant manifold that the system possesses when there is no asymmetry or noise. We will use ϵ to denote the transverse Lyapunov exponent for the periodic orbit that first becomes unstable in the transverse direction. In general, the largest Lyapunov exponent will not be equal to the bifurcation parameter of the system. However, they will be related by a smooth change of variables if the bifurcation parameter is also a normal parameter. Therefore, we will henceforth use ϵ to denote both the bifurcation parameter for the system and the largest Lyapunov exponent. This is consistent for the system in (1) near $\epsilon=0$. With this convention, we will have the bubbling transition at $\epsilon=0$.

We will use $h_{\|}$ to denote the largest Lyapunov exponent for the dynamics on the invariant manifold of the periodic orbit that mediates the bubbling transition. For the system in (1), the dynamics on the invariant manifold are governed by the $2x\mathrm{mod}1$ map, and consequently, $h_{\|}=\log 2$. The parameter q controls the amplitude of the asymmetry or the noise in the system.

As we discuss in Sec. I, our goal is to investigate the effect of adding asymmetry and noise to a system that would otherwise have an invariant manifold. In the presence of asymmetry or noise, the invariant manifold is destroyed. However, if $\epsilon<0$ and the amplitude of the asymmetry or the noise is sufficiently small, the attractor that exists on the manifold X for the noiseless symmetric case is replaced by an attractor that is restricted to a small neighborhood of X. In this case, the quantity of interest is Δ, the maximum deviation of the attractor from the manifold X. If coupled chaotic oscillators are operating in this parameter regime, the existence of such an attractor implies that the oscillators will eventually lock in the sense that after some time, the magnitude of the difference between the states of the oscillators due to noise or mismatch will not exceed Δ. Thus Δ represents the maximum deviation from synchrony.

If $\epsilon<0$ but the asymmetry or noise amplitude is sufficiently large or if $\epsilon>0$ and we have some asymmetry or noise in the system, every orbit that approaches the former invariant manifold will spend some length of time in its vicinity before it bursts away. The quantity of interest is τ, the average time spent in the vicinity of the invariant manifold.

We analyze the behavior of the model system in (1) in Secs. IV–VI, and we obtain results for Δ and τ in the vari-

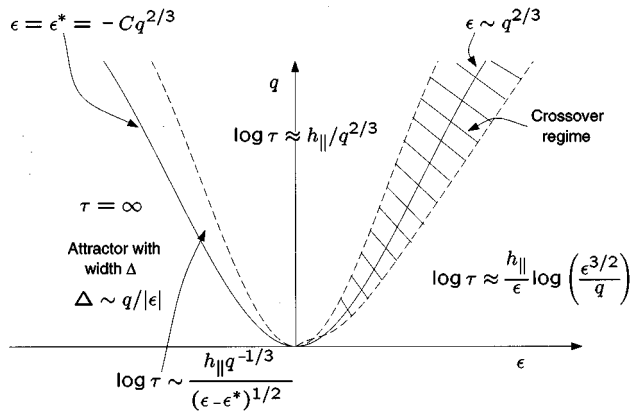

FIG. 6. A schematic representation of the results for the model with asymmetry. The results for the escape times in the various parameter regimes are shown.

ous regions of the parameter space (ϵ,q). We expect that these results are universal for a class of systems that display a bubbling transition. In particular, they apply to the model in Eqs. (1). These results are of interest in experiments and we summarize them in the remainder of this section. The results in Sec. III A are for the case of asymmetry (e.g., Eq. (1) with $\delta_1=1$, $\delta_2=0$), while the results in Sec. III B are for the case of noise [e.g., Eq. (1) with $\delta_1=0$, $\delta_2=1$].

A. Results for asymmetry

Figure 6 is a summary of the behavior of the model system in (1) for the case of asymmetry ($\delta_1=1$, $\delta_2=0$) in various regions in (ϵ,q) parameter space. There is a critical curve $\epsilon=\epsilon^*(q)\sim -q^{2/3}$, such that the system has an attractor in the vicinity of X for $\epsilon<\epsilon^*(q)$. In this region of parameter space, if the initial condition is close to $y=0$, y_n for the model in (1) eventually enters the region $|y|\leqslant\Delta$ and stays there. If $\epsilon>\epsilon^*$, almost every orbit that approaches $y=0$ eventually leaves the vicinity of $y=0$ after which it escapes rapidly to $y=\pm\infty$. The average time spent in the vicinity of the invariant manifold is given by τ which has different scaling behaviors in the different regions of parameter space. We discuss the results for systems with asymmetry in the various regions of the parameter space of Fig. 6 in the remainder of this section.

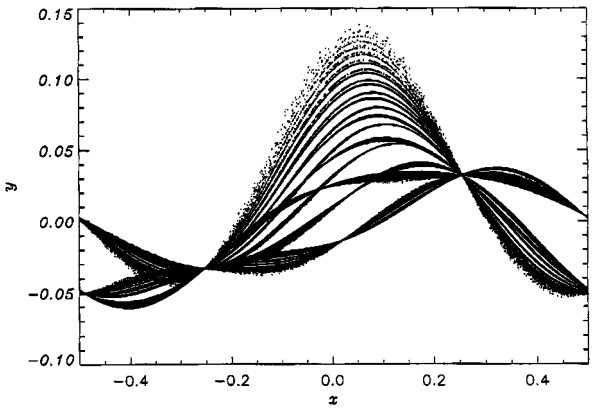

FIG. 7. An attractor for the system in (1) with $\delta_1=1$, $\delta_2=0$. The parameters have values $\epsilon=-0.1$ and $q=0.01$.

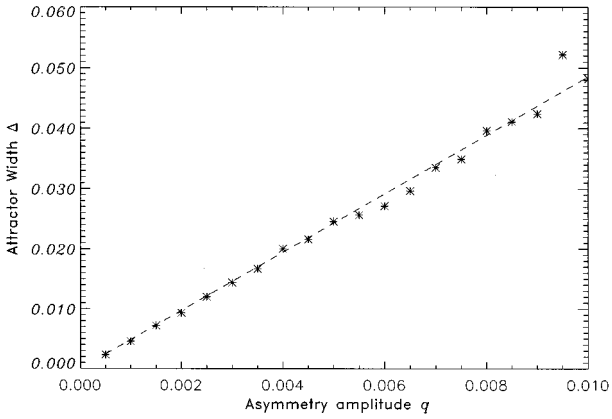

FIG. 8. The width of the attractor as a function of the asymmetry parameter. The dashed line is a fit.

(1) For $\epsilon<0$ and $q\neq 0$ sufficiently small, the system will have an attractor $\mathcal{B}$ in the vicinity of the ''ghost'' of the invariant manifold (the invariant manifold when there is no asymmetry or noise in the system). Figure 7 shows an attractor in the vicinity of $y=0$ for the system in Eq. (1) ($\delta_1=1$, $\delta_2=0$). The parameters have values $\epsilon=-0.1$, $q=0.01$.

The attractor $\mathcal{B}$ is confined to a layer of width Δ about $y=0$ where Δ scales [16] as

$$\Delta\sim q/|\epsilon|. \tag{8}$$

This is confirmed for the system (1) with $\delta_1=1$ and $\delta_2=0$ in Figs. 8 and 9. Figure 8 shows a plot of Δ as a function of q for with $\epsilon=-0.1$ and Fig. 9 shows a plot of Δ as a function of $1/|\epsilon|$ with $q=0.01$. For the data in Figs. 8 and 9, we determine Δ by following a typical orbit for 5 million iterations and taking the largest value of $|y_n|$. On both plots a fitted straight line that goes through the origin [prediction of Eq. (8)] is shown for comparison.

(2) For any $q\neq 0$, there exists $\epsilon^*(q)<0$, where $\epsilon^*(q)$ is a critical value of the parameter ϵ such that, as ϵ increases through $\epsilon^*(q)$, the attractor near X is destroyed by a crisis. For the system in (1) with the cubic nonlinearity, we have

$$\epsilon^*(q)\sim -|q|^{2/3}. \tag{9}$$

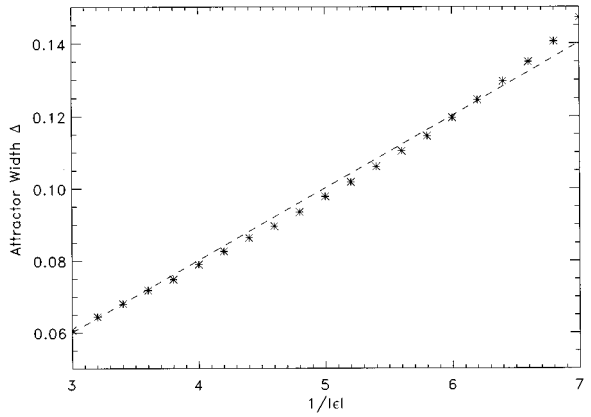

FIG. 9. The width of the attractor as a function of $1/|\epsilon|$. The dashed line is a straight line fit.

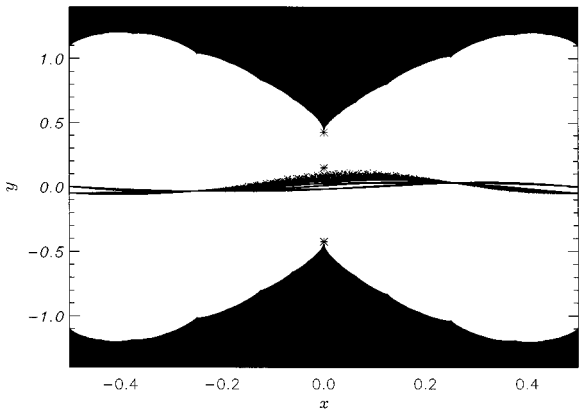

FIG. 10. The attractor and the basin boundaries for the system in (1) before the crisis. The parameters are $\delta_1=1$, $\delta_2=0$, $\epsilon=-0.1$, and $q=0.03$. The figure also shows the three period one points with $x=0$. As ϵ is increased, the saddle periodic point on the boundary of the attractor will merge with the upper unstable periodic point on the basin boundary.

Figure 10 shows the attractor $\mathcal{B}$ and the basins of attraction of the attractor at $y=\pm\infty$ (the black regions of Fig. 10) for the system in (1) with $\delta_1=1$, $\delta_2=0$ and ϵ close to, but less than ϵ^*. As $\epsilon\to\epsilon^*$, a saddle periodic orbit that lies on the boundary of the $\epsilon<\epsilon^*$ attractor merges with a repelling periodic orbit on the basin boundary. This phenomenon has been studied more generally in [17]. As ϵ increases through ϵ^*, the attractor $\mathcal{B}$ is destroyed by this boundary crisis and is replaced by a chaotic transient. In this case, almost all the orbits eventually end up at $y=\pm\infty$.

(3) For $\epsilon>\epsilon^*$ and $q\neq 0$, every orbit (except for a set of Lebesgue measure zero) eventually leaves any given open neighborhood $\mathcal{O}$ of the ghost manifold X. Figure 11 is a plot of the logarithm of $N(n)$, the number of orbits that remain in $|y|<1.5$ after n steps for the map in (1). This plot is obtained by randomly sprinkling 10 000 initial conditions on the line $y=0$ and following the orbits generated by these initial conditions. From the plot, we see that

$$N(n)\sim N_0 e^{-n/\tau}, \tag{10}$$

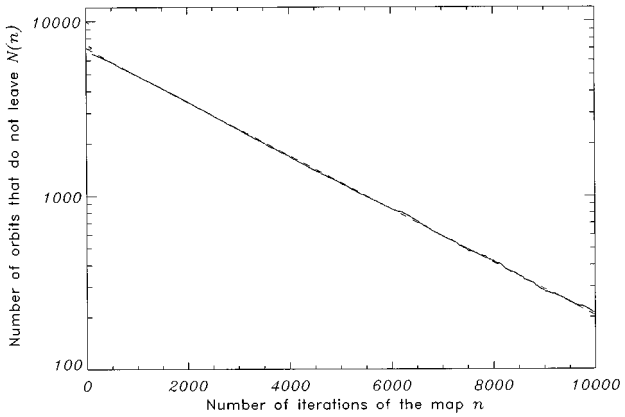

FIG. 11. A plot of the number of orbits that are left in the region $|y|<1.5$ as a function of the number of iterations of the map.

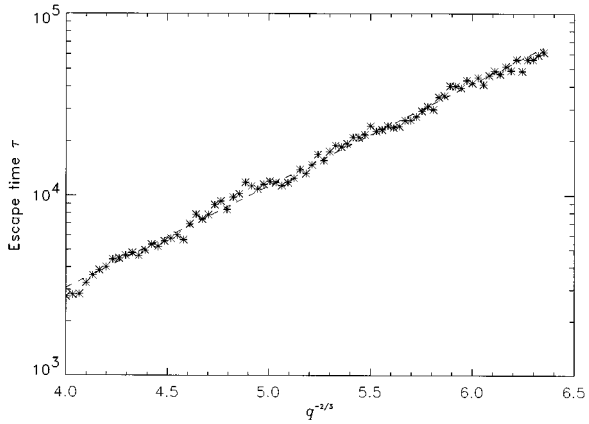

FIG. 12. This plot shows the escape time as a function of $q^{-2/3}$ when $|\epsilon|\ll q^{2/3}$. The parameter ϵ is 0.01. The dashed line is a fit.

after an initial transient. We will call the time τ the *escape time*. τ is of the order of the average length of the chaotic transient that follows the ''ghost'' of the attractor $\mathcal{B}$.

(4) For $|\epsilon|\ll q^{2/3}$, we obtain

$$\log\tau\sim\frac{h_\parallel}{q^{2/3}}. \tag{11}$$

This result is also obtained in [18] for the special case $\epsilon=0$. Figure 12 is a plot of $\log\tau$ as a function of $1/q^{2/3}$ for $\delta_1=1$, $\delta_2=0$ and $\epsilon=0.01$. The data lie along a straight line which is in agreement with the predicted scaling.

(5) For $\epsilon>0$ and $\epsilon\gg q^{2/3}$, we have [19]

$$\log\tau\simeq\frac{h_\parallel}{|\epsilon|}\log\left(\frac{\epsilon^{3/2}}{q}\right). \tag{12}$$

Figure 13 shows a plot of $\log\tau$ as a function of $\log q$ for the model in (1) with $\delta_1=1$, $\delta_2=0$ and $\epsilon=0.2$. The dashed line has the theoretically predicted slope of $-h_\parallel/\epsilon$ and the data agree well with the predicted scaling.

(6) For ϵ close to, but larger than ϵ^*, the escape time is given by

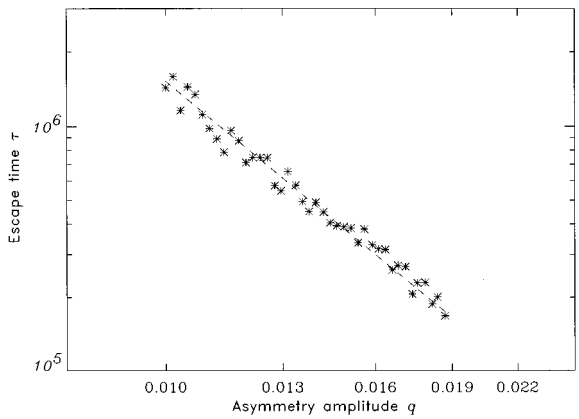

FIG. 13. This plot shows the escape time as a function of the asymmetry amplitude q when $\epsilon/q\gg 1$. The parameter ϵ is 0.2 and both axes are on log scales. The dashed line has a slope equal to $-h_\parallel/\epsilon$, which is the theoretical prediction.

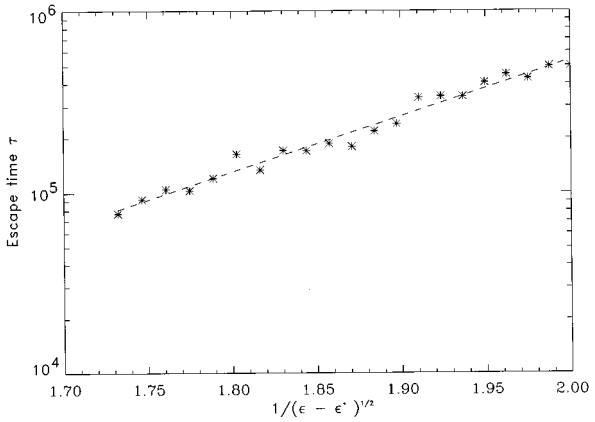

FIG. 14. This plot shows the scaling of the escape time as a function of the largest transverse Lyapunov exponent ϵ when ϵ is close to its critical value ϵ^*. The dashed line is a fit.

$$\log\tau \sim \frac{h_\parallel |\epsilon^*|^{-1/2}}{|\epsilon-\epsilon^*|^{1/2}}. \tag{13}$$

The dependence $\log\tau \sim |\epsilon-\epsilon^*|^{-1/2}$ for a constant q can be viewed as a consequence of the result derived in [17] where the authors study the chaotic transient time due to an attractor that is destroyed by a crisis that is mediated by the coalescence of a saddle periodic orbit on the attractor with a repellor periodic orbit on the basin boundary. (This is the relevant type of crisis in our case [see Fig. 10], and is called an unstable-unstable pair crisis [17]). Equation (13) shows that as we approach the critical line $\epsilon=\epsilon^*$ at constant q by decreasing ϵ, we have that $\log\tau$ diverges as $|\epsilon-\epsilon^*|^{-1/2}$. Similarly, as we approach the critical line at constant ϵ by decreasing q, We have that $\log\tau$ diverges as $|q-q^*(\epsilon)|^{-1/2}$ where $q^*(\epsilon)\sim(-\epsilon)^{3/2}$. Figure 14 shows a plot of $\log\tau$ as a function of $1/|\epsilon-\epsilon^*|^{1/2}$ for a constant value of q.

The scaling results in items 1–6 of this section are summarized in Fig. 6. Note that the results (11) and (12) agree in the crossover regime (shown hatched in the figure). Also note that (13) and (12) become the same in the region to the right of the dashed line which is placed at $\epsilon=(3/4)\epsilon^*$ [the factor 3/4 is somewhat arbitrary and can be replaced by any positive number $\alpha<1$ such that $1-\alpha\sim O(1)$].

B. Results for noise

Figure 15 is a summary of the behavior of the model system in (1) for the case of noise ($\delta_1=0$, $\delta_2=1$) in various regions in (ϵ,q) parameter space. In the region $\epsilon<\epsilon^{**}(q)\sim -q$ the behavior of the system depends on the exact details of the noise distribution. We refer to this region as the non-universal regime. In $\epsilon>\epsilon^{**}$ on the other hand, results depending only on the noise variance q and otherwise independent of the noise distribution can be obtained. If $\epsilon>\epsilon^{**}$, almost every orbit that approaches $y=0$ eventually leaves the vicinity of $y=0$ after which it escapes rapidly to $y=\pm\infty$. The average time spent in the vicinity of the invariant manifold is given by τ which again has different scaling behaviors in the different regions of parameter space. We discuss these results in the remainder of this section.

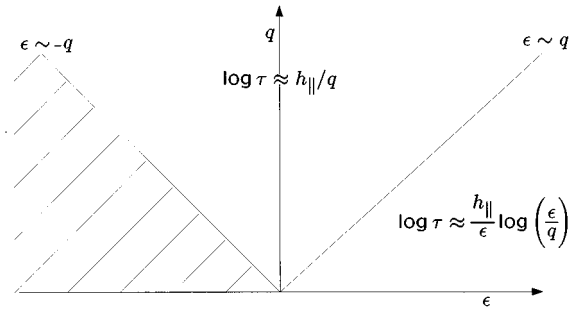

FIG. 15. A schematic representation of the results for the model with additive noise. The results for the escape times in the various parameter regimes are shown.

(1) For $|\epsilon|\ll q$, we have the result

$$\log\tau \sim \frac{h_\parallel}{q}. \tag{14}$$

Figure 16 is a plot of the logarithm of the escape time as a function of $1/q$ for the system in (1) with $\delta_1=0$, $\delta_2=1$ and $\epsilon=0.01$. The dashed line is a fit and the data lie along this line in agreement with the predicted scaling.

(2) For ϵ positive and $\epsilon\gg q$, we obtain

$$\log\tau \simeq \frac{h_\parallel}{\epsilon}\log(\epsilon/q). \tag{15}$$

Figure 17 is a plot of $\log\tau$ as a function of $\log q$ with $\epsilon=0.2$. The dashed line corresponds to the theoretical slope of $-h_\parallel/\epsilon$ and the data agree with the prediction.

(3) The results in items 1 and 2 above are universal in the sense that they depend only on the noise variance q^2 and not on the form of the noise probability distribution function. Our calculations (not given here) lead us to conjecture that for $\epsilon\ll -q$ this universality does not hold, and, in particular the form of the low probability tail of the distribution is important. Thus, qualitatively different scaling may result, for example, for Gaussian and bounded noise distributions.

The scaling results in items 1 and 2 of this section for systems with noise are summarized in Fig. 15.

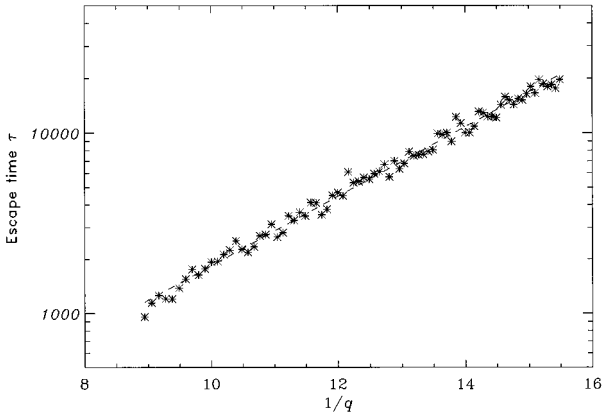

FIG. 16. This plot shows the escape time as a function of $1/q$ where q is the noise amplitude and $\epsilon/q\ll 1$. The parameter ϵ is 0.01. The dashed line is a fit.

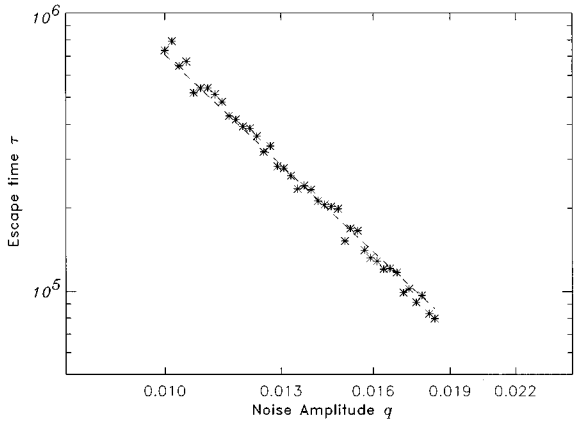

FIG. 17. This plot shows the escape time as a function of the noise amplitude q when $\epsilon/q \gg 1$. The parameter ϵ is 0.2. Both the axes are on log scales. The dashed line has the theoretically predicted slope $-h_{\|}/\epsilon$.

When noise and asymmetry are both present, the escape time may be estimated as

$$\tau = \min(\tau_a, \tau_n), \tag{16}$$

where τ_a and τ_n are the escape times due to the asymmetry and the noise respectively. We will derive and discuss the results stated in Secs. III A and III B in Secs. IV–VI.

It is noteworthy that our scalings and numerical results indicate remarkably long escape times even when ϵ and q are not tiny [e.g., in Fig. 14 the escape time τ ranges from 10^5 to 10^6 for $|(\epsilon-\epsilon^*)/\epsilon^*| \sim 0.3$].

IV. ESCAPE TIME

We will now obtain a formula for the escape time for the map in (1). If we are close to the bubbling transition, only points whose x coordinates are very close to 0 (the fixed point of the $2x$mod1 map that mediates the bubbling transition) are repelled away from X, the ghost of the invariant manifold (X is the set $y=0, 0 \leqslant x \leqslant 1$). All other points experience average attraction toward X, until they land close to $x=0$. In particular, there will exist an open set $\mathcal{U} \subset X$ containing 0 such that if x is outside $\mathcal{U}$, an orbit starting at (x,y) is attracted towards the ghost of the invariant manifold in the next step and an orbit starting at (x,y) with $x \in \mathcal{U}$ is repelled away from the invariant manifold in the next step. Therefore, for an orbit starting at $(x,0)$ to get to $y=y_{max}$ without returning to the vicinity of X, we need that $[x, x_1, x_2, \ldots, x_l] \in \mathcal{U}$, where l is the number of steps it takes to get to y_{max}.

Since the dynamical system (1) is a continuous map on the phase space, the number of steps required to get to y_{max} is approximately the same as the number of steps that an orbit starting at (0,0) takes to get to y_{max}. Let $\overline{n}$ be the number of steps that an orbit starting at (0,0) takes to get to y_{max}. Then, $l \approx \overline{n}$.

If we want $[x, x_1, x_2, \ldots, x_l] \in \mathcal{U}$, then x should lie in an interval O whose width W_0 is given by

$$W_0 = \exp(-h_{\|}\overline{n}) W(\mathcal{U}), \tag{17}$$

where $W(\mathcal{U})$ is the width of $\mathcal{U}$. The escape time is the expected time for a typical orbit of the $2x$mod1 map to end up in O. Consequently,

$$\tau \sim 1/W_0, \tag{18}$$

and this yields

$$\tau \sim [W(\mathcal{U})]^{-1} \exp(\overline{nh}_{\|}). \tag{19}$$

It can be shown that the $\overline{n}$ dependence of $W(\mathcal{U})$ is very much weaker than the exponential dependence, $\exp(\overline{nh}_{\|})$ (e.g., the calculation in Sec. VI B implies $W(\mathcal{U}) \sim O(1)$ when $(\epsilon-\epsilon^*)/|\epsilon^*|$ is not very small). Consequently, for $\overline{n} \gg 1$ we have

$$\log \tau \sim \overline{nh}_{\|}. \tag{20}$$

V. ASYMMETRY

A. Attractor for $\epsilon < \epsilon^*$

For the 2D map in Eq. (1) we can demonstrate the results in item 1 of Sec. III A, i.e., we can show that there exists an attractor $\mathcal{B}$ in the vicinity of the ghost of the invariant manifold ($y=0$) and this attractor is confined to a layer of width Δ which is given by Eq. (8). From Eq. (1), we have

$$\begin{aligned} |y_{n+1}| &= |\lambda(x_n) y_n + q \sin(2\pi x_n + \gamma) + y_n^3| \\ &\leqslant |\lambda(x_n)||y_n| + q + |y_n|^3, \end{aligned} \tag{21}$$

where $\lambda(x)$ is given by Eq. (4). We are considering the case $\epsilon < 0$. Consequently, $|\lambda(x)| \leqslant 1 - |\epsilon|$. Also, we assume that $|y_n|^3 \leqslant q/2$. This assumption is verified later. With this assumption, for $|y_n| \leqslant 3q/(2|\epsilon|)$, we have

$$|y_{n+1}| \leqslant 3q/(2|\epsilon|). \tag{22}$$

This implies every orbit for the system in (1) that starts off near the invariant manifold is confined to a layer of width $\Delta \approx 3q/(2|\epsilon|)$ [this is Eq. (8)]. Also, because the set $[0,1] \times [-\Delta, \Delta]$ is compact, every infinite sequence of points has at least one limit point. This implies the existence of an attractor $\mathcal{B}$, for the dynamical system in (1), within this set.

In order that our assumption that $y_n^3 \leqslant q/2$ hold, since $|y| < \Delta \leqslant 3q/2|\epsilon|$, we require $(q/2)^2 < |\epsilon/3|^3$. This is satisfied when $\epsilon < \epsilon^* = -3(q/2)^{2/3}$, which is also the exact result for ϵ^* in (26). Consequently, we have an attractor for $\epsilon < \epsilon^*$ and it is confined to a band of width $\Delta \sim q/|\epsilon|$.

B. Escape times

We consider the 2D map in Eq. (1) with $\delta_1 = 1$ and $\delta_2 = 0$. The periodic orbit of the $2x$mod1 map that is the most unstable in the transverse direction is the fixed point at $x=0$. In the vicinity of $x=0$, the equation for y_n reduces to

$$y_{n+1} = y_n^3 + (1+\epsilon) y_n + q_0, \tag{23}$$

where $q_0 = q \sin(\gamma)$.

If y_p is a fixed point of Eq. (23), then the point $(0,y_p)$ is a fixed point (periodic point with period 1), of the map in (1). The fixed points of Eq. (23) are given by the solutions of

$$y_p^3+\epsilon y_p+q_0=0. \tag{24}$$

For the cubic equation in (24) to have three real roots, we need that

$$y_{mx}y_{mn}<0, \tag{25}$$

where y_{mx} and y_{mn} are the local maximum and minimum for the cubic polynomial in (24). This yields the condition

$$\epsilon<\epsilon^*=-3\left|\frac{q_0}{2}\right|^{2/3}, \tag{26}$$

which is the result in item 2 of Sec. III A.

If $\epsilon<\epsilon^*$, we have three real roots for Eq. (24). Therefore, we have three fixed points. Two of these fixed points are unstable but the third fixed point is stable. Therefore, an orbit starting at (0,0) will not escape to $y=\infty$. It will instead end up at the fixed point that is stable. By the argument in Sec. IV, this implies that none of the orbits that start off near the manifold $y=0$ make it out to $y=\pm\infty$. They instead end up on an attractor $\mathcal{B}$ in the vicinity of $y=0$. Further, this attractor is a topolgical attractor and the stable fixed point of Eq. (23) is embedded in it. The two unstable fixed points of Eq. (23) lie on the basin boundary of the attractor at $y=\pm\infty$. This demonstrates the results in item 2 of Sec. III A. This result is illustrated in Fig. 10. The fixed points in the figure have been calculated by numerically solving Eq. (24).

For $\epsilon>\epsilon^*$, Eq. (24) has only one real root. The fixed point corresponding to this root is unstable. Therefore, an orbit starting at (0,0) will eventually end up at $y=\infty$. Consequently, every orbit starting in the vicinity of the invariant manifold will eventually escape. As $\epsilon\to\epsilon^*$, the stable fixed point on the attractor $\mathcal{B}$ will merge with the unstable fixed point on the boundary of the basin of the attractor at $y=\pm\infty$ as the two roots of the cubic in (24) merge. This is a boundary crisis as a periodic point in the attractor merges with an unstable periodic point on the basin boundary. The attractor $\mathcal{B}$ is therefore destroyed in a crisis and is replaced by a chaotic transient. We expect that this behavior is generic in systems with asymmetry near the bubbling transition.

By the argument in Sec. IV, it suffices to consider an orbit starting at (0,0) to evaluate the escape time for $\epsilon>\epsilon^*$. Because of the y_n^3 nonlinearity, there exists a y_{max} such that if $|y_n|>y_{max}$, the orbit rapidly goes to the attractor at $\pm\infty$ independent of x_n. Let $\overline{n}$ be the number of steps that an orbit starting at (0,0) takes to get to $(0,y_{max})$. If $q\ll1$ and $\epsilon\ll1$, the number of steps required is large, i.e., $\overline{n}\gg1$. In that case, we can replace Eq. (23) by the differential equation

$$\frac{dy(n)}{dn}=y^3+\epsilon y+q_0. \tag{27}$$

We can then evaluate $\overline{n}$ by

$$\overline{n}\approx\int_0^{y_{max}}\frac{dy}{y^3+\epsilon y+q_0}, \tag{28}$$

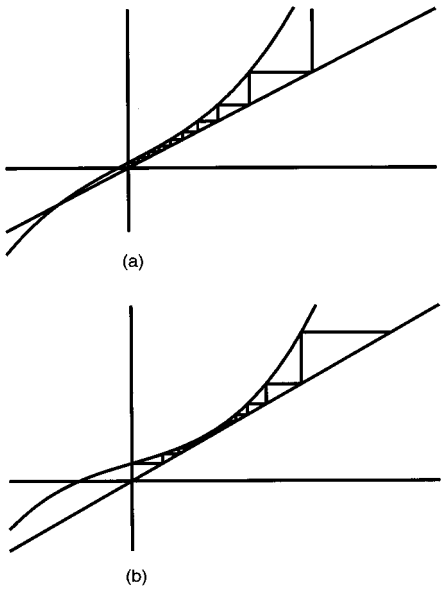

FIG. 18. These figures show the y coordinates of orbits that have initial condition (0,0) and escape to infinity. (a) $\epsilon>0$. In this case, most of the steps needed to get away from the origin are in the region where the y^3 term does not exceed the ϵy or the q_0 term. (b) ϵ is close to ϵ^*. In this case, most of the steps are in the vicinity of the ''ghost'' fixed point at $|\epsilon^*/3|^{1/2}$. In this case, Eq. (34) is the appropriate expression for $\overline{n}$.

and the escape time is given by Eq. (20). Let $a(\epsilon,q)$ be a cutoff such that for $y<a(\epsilon,q)$, we can neglect the y^3 in the denominator of the integrand. Therefore, we have

$$a(\epsilon,q)=\max(\epsilon^{1/2},q_0^{1/3}). \tag{29}$$

Consequently, the number of steps needed to get from (0,0) to $(0,y_{max})$ is given by

$$\overline{n}\approx\int_0^{a(\epsilon,q)}\frac{dy}{\epsilon y+q_0}+\int_{a(\epsilon,q)}^{y_{max}}\frac{dy}{y^3}. \tag{30}$$

This yields

$$\overline{n}\approx\frac{\log[1+a(\epsilon,q)\epsilon/q_0]}{\epsilon}+\frac{1}{2[a(\epsilon,q)]^2}. \tag{31}$$

Using this equation with the results in Eq. (20) and (29), we obtain the scaling results in items 4 and 5 of Sec. III A. Figure 18(a) shows the y coordinate of an orbit starting at (0,0) for $\epsilon>0$. Note that in this case, most of the steps required to get to $y=y_{max}$ are in the region where the y^3 nonlinearity can be neglected. For $\epsilon=\epsilon^*$, the cubic in (24) has a repeated root at $y=|\epsilon/3|^{1/2}$ which is in the range of integration in (28). For ϵ close to but larger than ϵ^*, the cubic in the denominator of the integrand in (28) has a quadratic minimum at $y=|\epsilon/3|^{1/2}$ and most of the steps that an orbit from (0,0) takes to get to $(0,y_{max})$ are in the vicinity of this point [see Fig. 18(b)]. In this case (31) is not valid and a separate analysis is required. Near $y=|\epsilon/3|^{1/2}$ we have

$$y^3-|\epsilon|y+q_0=(y+2|\epsilon/3|^{1/2})(y-|\epsilon/3|^{1/2})^2+(q_0-2|\epsilon/3|^{3/2}). \tag{32}$$

Therefore, we obtain

$$\overline{n} \approx \int_0^{y_{max}} \frac{dy}{y^3+\epsilon y+q_0}$$

$$\approx \frac{1}{(3|\epsilon^*|)^{1/2}} \int_0^{y_{max}} \frac{dy}{(y-|\epsilon/3|^{1/2})^2+|\epsilon-\epsilon^*|}, \quad (33)$$

where ϵ^* is given by Eq. (26). If ϵ is close to ϵ^*, so that $|\epsilon/3| \gg |\epsilon-\epsilon^*|$ and q is small so that $y_{max} \gg q$, we have,

$$\overline{n} \approx \frac{\pi}{(3|\epsilon^*|)^{1/2}|\epsilon-\epsilon^*|^{1/2}}. \quad (34)$$

Using Eq. (20) we obtain the result

$$\log\tau \sim h_{\|}|\epsilon^*|^{-1/2}/|\epsilon-\epsilon^*|^{1/2}, \quad (35)$$

which is the result Eq. (13) in item 6 of Sec. III A.

A more accurate expression can be obtained by using (19) to write $\log\tau \approx \overline{nh}_{\|} - \log W(\mathcal{U})$ in place of (20). Although the term $\log W(\mathcal{U})$ is of higher order as compared to $\overline{nh}_{\|}$, its inclusion may improve the accuracy of the result in some cases. To estimate $W(\mathcal{U})$ we write $\lambda(x)$ from (4) as

$$\lambda(x) = 1+\epsilon-(r/2)x^2+O(x^4).$$

We note that both ϵ and $-(r/2)x^2$ have similar effects in that they cause $\lambda(x)$ to deviate from 1. Thus, if $(r/2)x^2$ exceeds $[\epsilon-\epsilon^*(q)]$, the orbit will return to the vicinity of the invariant manifold. Hence we have

$$W(\mathcal{U}) \sim |\epsilon-\epsilon^*(q)|^{1/2}$$

and (35) is replaced by

$$\log[|\epsilon-\epsilon^*|^{1/2}\tau] \sim h_{\|}|\epsilon^*|^{1/2}/|\epsilon-\epsilon^*|^{1/2}. \quad (36)$$

[If $\log|\epsilon-\epsilon^*|^{-1/2}$ is small compared to the right-hand side, then (36) reduces to (35). This is valid for the range plotted in Fig. 17.]

VI. NOISE

A. Escape times

In this section we will calculate the escape time for the model in (1) with $\delta_1 = 0$ and $\delta_2 = 1$. The escape time is again given by (20) where $\overline{n}$ is the typical number of steps that an orbit starting at (0,0) takes to get to $|y| > y_{max}$.

An orbit starting at (0,0) is given by $x_n = 0$, and

$$y_{n+1} = (1+\epsilon)y_n + y_n^3 + q\nu_n. \quad (37)$$

If $\overline{n} \gg 1$, we can replace the difference equation for y_n by the (stochastic) differential equation

$$\frac{dy}{dt} = \epsilon y + q\nu(t) + y^3, \quad (38)$$

where $\nu(t)$ is a continuous time noise process with $E[\nu(t)\nu(t')] = \delta(t-t')$.

If we are close to the invariant manifold, we can neglect the y^3 nonlinearity in (38). Let $a(\epsilon,q)$ be a cutoff such that for $y < a(\epsilon,q)$, we can neglect the y^3 nonlinearity and for $y > a(\epsilon,q)$, the only important term is the y^3. Then, we have

$$\overline{n} = n_1 + n_2, \quad (39)$$

where n_1 is the typical number of steps needed to get from (0,0) to $(0,a(\epsilon,q))$ and n_2 is the typical number of steps needed to get from $(0,a(\epsilon,q))$ to $(0,y_{max})$. We can evaluate n_2 by

$$n_2 \approx \int_{a(\epsilon,q)}^{y_{max}} \frac{dy}{y^3} \approx \frac{1}{2[a(\epsilon,q)]^2}. \quad (40)$$

We will now evaluate n_1. For $y < a(\epsilon,q)$, Eq. (38) reduces to

$$\frac{dy(t)}{dt} = \epsilon y + q\nu(t). \quad (41)$$

We can solve this equation to get

$$y(t) = q\int_0^t \nu(t')e^{\epsilon(t-t')}dt'. \quad (42)$$

From this, we get

$$E[[y(t)]^2] = q^2\int_0^t\int_0^t E[\nu(t')\nu(t'')]e^{\epsilon(t-t')}e^{\epsilon(t-t'')}dt'dt''. \quad (43)$$

Therefore, we obtain

$$E[[y(t)]^2] = \frac{q^2}{2\epsilon}(e^{2\epsilon t}-1). \quad (44)$$

If $\epsilon > 0$, the variance of $y(t)$ increases without bound and it will eventually become greater than $[a(\epsilon,q)]^2$ for any $a(\epsilon,q)$. The time taken for the variance to become a^2 is n_1. Therefore,

$$n_1 = \frac{\log\{1+2\epsilon[a(\epsilon,q)]^2/q^2\}}{2\epsilon}. \quad (45)$$

If $\epsilon < 0$, the variance of $y(t)$ grows till a time $t_0 \sim 1/|\epsilon|$ when it has a value $q^2/2|\epsilon|$. Now, if $q^2/2|\epsilon| \gg [a(\epsilon,q)]^2$, n_1 is again given by the expression in (45).

The cutoff $a(\epsilon,q)$ is determined by the following argument. Assume that we have an ensemble of N orbits all starting at (0,0). Then, after a time n_1, the y coordinates of the orbits have a distribution with a variance close to $a(\epsilon,q)^2$. If we wait for another $m \ll n_1$ steps, the average drift due to the ϵy term in (38) is

$$\Delta_1 \approx m|\epsilon|a(\epsilon,q). \quad (46)$$

The change in the standard deviation of the y coordinates of the orbits in the ensemble due to the noise (denoted by Δ_2) can be estimated from the linear increase of the variance with time,

$$(a+\Delta_2)^2 - a^2 = mq^2, \quad (47)$$

appropriate to the random walk

$$\frac{dy}{dt}=q\nu(t). \tag{48}$$

We therefore obtain

$$\Delta_2\approx mq^2/a(\epsilon,q). \tag{49}$$

The average drift due to the y^3 nonlinearity is

$$\Delta_3\approx ma(\epsilon,q)^3. \tag{50}$$

The cutoff $a(\epsilon,q)$ is determined by requiring that

$$\Delta_3\leqslant\max(\Delta_1,\Delta_2). \tag{51}$$

From this, we obtain

$$a(\epsilon,q)\sim\max(|\epsilon|^{1/2},q^{1/2}). \tag{52}$$

Equations (52), (45), (40), (39), and (20) together yield the results in items 1 and 2 of Sec. III B.

B. Noise in the x direction

We consider now the effect of adding noise to the dynamics of x in our model (1), as in Eq. (2). Our estimates of the escape time have been based on the premise that in order to escape, the x coordinate of the trajectory must stay within a neighborhood $\mathcal{U}$ of the fixed point at 0 for $l\approx\overline{n}$ iterates, and that to do so x must fall within an interval of length approximately W_0 given by Eq. (17). We claim that Eq. (17) continues to hold as long as the noise strength $\overline{q}$ (which we assume is of the same order as q) is small compared with the width $W(\mathcal{U})$ of $\mathcal{U}$.

The width of $\mathcal{U}$ can be estimated as follows. The neighborhood $\mathcal{U}$ is determined by requiring that if $x_0,x_1,\ldots,x_l\in\mathcal{U}$, the orbit closely follows an orbit starting at (0,0). For this to hold over l steps, we need

$$\prod_{i=1}^{l}\lambda(x_i)\approx[\lambda(0)]^l, \tag{53}$$

where $\lambda(x)$ is the transverse expansion factor defined in (4). From Eq. (4), we have

$$\lambda(x)=1+\epsilon-\frac{r}{2}x^2+O(x^4)\approx\lambda(0)\exp(-rx^2/2). \tag{54}$$

For $\overline{q}\ll W(\mathcal{U})$ we can neglect the noise perturbations in Eq. (2). In this case,

$$x_i\approx 2^i x_0. \tag{55}$$

Therefore

$$\prod_{i=1}^{l}\lambda(x_i)\approx[\lambda(0)]^l\exp\left(-\frac{r}{2}\sum_{i=0}^{l}x_i^2\right). \tag{56}$$

The set $\mathcal{U}$ is therefore determined by requiring that,

$$\sum_{i=0}^{l}x_i^2\approx 4x_l^2/3\sim O(1). \tag{57}$$

Consequently, we have

$$W(\mathcal{U})\sim O(1). \tag{58}$$

For $\overline{q}\to 0$, we have,

$$\overline{q}\ll W(\mathcal{U}). \tag{59}$$

Based on our claim above that Eq. (17) is valid when $\overline{q}\ll W(\mathcal{U})$, the noise in the x direction does not affect the scaling results for the escape time in Sec. III B. We now verify this claim.

Let an orbit starting at $(x_0,0)$ escape without returning to the vicinity of $y=0$. Then, $x_0,x_1,\ldots,x_l$ lie in $\mathcal{U}$. Assume that the noise perturbations $q\nu_0,q\nu_1,\ldots,q\nu_{l-1}$ have been chosen. Then since $x_l\in\mathcal{U}$, its preimage x_{l-1} must lie in a set $\mathcal{U}_{l-1}$ of half the width of $\mathcal{U}$; the location of $\mathcal{U}_{l-1}$ is not centered at 0, but is shifted by half the noise perturbation $q\nu_{l-1}$. Since the size of this translation is of order $\overline{q}$, it is small compared with $W(\mathcal{U})$, and thus $\mathcal{U}_{l-1}$ is inside $\mathcal{U}$. Likewise x_{l-2} must lie in a set $\mathcal{U}_{l-2}$ of width half that of $\mathcal{U}_{l-1}$, and $\mathcal{U}_{l-2}$ is contained in $\mathcal{U}$, and so on. We conclude that x_0 must lie in a set $\mathcal{U}_0$ of width W_0, where W_0 is given by Eq. (17) with $h_\parallel=\log 2$.

By this argument, we expect that the results we derive using the map in (1), which does not have noise in the x direction, are also valid for more realistic models which have a more isotropic noise. We also note that this argument generalizes beyond the $2x$ mod1 map.

VII. INTERMITTENT BURSTING

As we discuss in Sec. I, for a system that displays the bubbling transition, there are two cases of interest. In the first case, there exist attractors in the phase space off the invariant manifold. This situation leads to the occurrence of riddled basins and it has been considered in Secs. III–VI. In the other case, the symmetric noiseless system has no attractors other than the one in the invariant manifold. In this situation, a small noise or asymmetry will cause the system to burst away from the invariant manifold intermittently. The mechanism of bursting is the same as the mechanism for the escape of orbits in the first case. In this situation, however, almost every orbit eventually returns to the vicinity of the symmetric noiseless invariant manifold because there are no attractors off the invariant manifold. This orbit will then spend a length of time in the vicinity of the invariant manifold before it again bursts away.

The transition to bursting behavior as ϵ is increased through ϵ^* can be of the following two types:

(i) As ϵ is increased through ϵ^*, the bursts appear with an amplitude that increases continuously from Δ, the width of the attractor for $\epsilon<\epsilon^*$. We will call this type of bifurcation a *soft transition*.

(ii) As ϵ is increased through ϵ^*, the bursts appear with a large amplitude. The maximum deviation from the invariant manifold changes discontinuously from $O(\Delta)$ for $\epsilon<\epsilon^*$ to $O(1)$ for $\epsilon>\epsilon^*$. We will call this type of bifurcation a *hard transition*.

The map in (1) has attractors at $\pm\infty$ that are off $y=0$, the invariant manifold for the symmetric noiseless system. We can modify the map in (1) in two ways to remove these

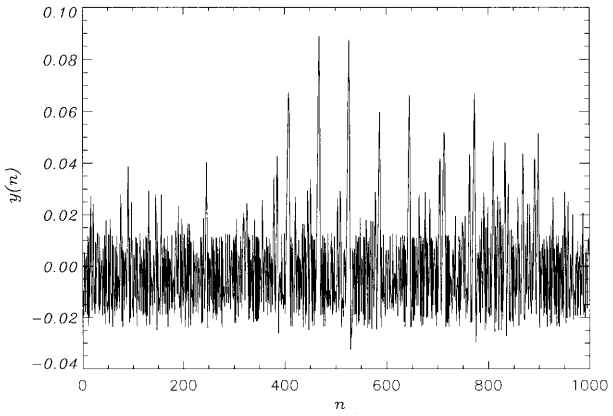

FIG. 19. A typical time series of y_n for the system in (60). The system spends most of its time in the vicinity of the ''ghost'' manifold ($y=0$) but it bursts away intermittently.

attractors. One way is to replace the $+y_n^3$ nonlinearity that drives orbits away from $y=0$ by the confining $-y_n^3$ nonlinearity. In this case, we have the dynamical system

$$x_{n+1}=2x_n \mod 1,$$

$$y_{n+1}=\{1+\epsilon-r[1-\cos(2\pi x_n)]\}y_n+q\sin(2\pi x_n+\gamma)-y_n^3. \tag{60}$$

Figure 19 is a typical time series of y_n generated by the model in (60) with $\epsilon-\epsilon^*$ small and positive. The system spends most of the time in the vicinity of the invariant manifold (the laminar phases) but these periods are interrupted by short bursts where the system leaves the vicinity of the invariant manifold.

The $-y_n^3$ nonlinearity in (60) ensures that, for some range of parameters, orbits starting near $y=0$ are bounded. In this parameter range, every orbit is bounded to a set $|y|\leqslant y_{max}$, where, from (60) with $x=0$, y_{max} satisfies

$$y_{max}=(1+\epsilon)y_{max}+q_0-y_{max}^3. \tag{61}$$

Every burst has a height less than or equal to y_{max} and y_{max} is a continuous function of ϵ. Therefore, the transiton at $\epsilon=\epsilon^*$ for the map in (60) is a soft transition.

We can also remove the attractors at $y=\pm\infty$ for the map in (1) if we retain the $+y_n^3$ nonlinearity but we modify the map in the region far from $y=0$ [i.e., $|y|\sim O(1)$] in such a way that the orbit remains bounded. In this case, for $\epsilon>\epsilon^*$, an orbit that leaves the vicinity of the former noiseless symmetric invariant manifold is pushed further away by the y^3 nonlinearity. However, when it gets to $|y|\sim O(1)$ it can go no further. In this situation, as ϵ is increased through ϵ^*, the bursts appear with a large [i.e., $O(1)$] amplitude; that is, there is a hard transition.

We will define the laminar phases to be the set of time indices n such that $|y_n|\leqslant y_0$, for some chosen threshold y_0 where y_0 is small compared to the maximum burst size. In the context of synchronized oscillators, y_0 is the maximum deviation from synchronization that is acceptable. The mechanism for this bursting is the same as the mechanism for the escape of orbits in the riddled basin case. Consequently, a laminar phase is analogous to the chaotic transient in the vicinity of the ghost attractor that was discussed in Secs. III–VI. Therefore, from the results of the earlier sections, the duration of the laminar phases is exponentially distributed. The probability density $P(t)$, that a laminar phase has a length t is given by

$$P(t)\sim e^{-t/\tau}, \tag{62}$$

where τ is the average interburst interval.

All these bursts occur when the x coordinates of the orbit are near those of the periodic orbit that mediates the bubbling transition. Let $\overline{n}$ denote the typical number of steps that an orbit starting at $(0,0)$ takes to get to $(0,y_0)$. Then,

$$\overline{n}\approx\int_0^{y_0}\frac{dy}{q_0+\epsilon y+\eta y^3}, \tag{63}$$

where $\eta=1$ for the hard transition and $\eta=-1$ for the soft transition. By our earlier arguments, τ, the average length of the laminar phase scales according to Eq. (20).

VIII. SYNCHRONIZED OSCILLATORS WITH ASYMMETRIC COUPLING

As discussed at the end of Sec. II, a situation of experimental interest is the synchronization of electrical oscillators. This is typically done by making the oscillators nearly identical and electrically coupling them together. This coupling may or may not be symmetric. In the case of symmetric coupling, our previous considerations of Secs. II–VII apply. In the case of asymmetric coupling, the basic model Eq. (1) must be modified. In particular, as discussed in Sec. II, the lowest order nonlinearity is y_n^2 rather than y_n^3. In this section we consider the asymmetric coupling case. In the noiseless case, the y-equation of (1) is replaced by

$$y_{n+1}=\{1+\epsilon-r[1-\cos(2\pi x_n)]\}y_n+y_n^2+q\sin(2\pi x_n+\gamma). \tag{64}$$

The nonlinearity is written as $+y_n^2$; changing $+y_n^2$ to $-y_n^2$ is equivalent to changing the sign of q. As we discuss in the preceding section, we can have both a hard and a soft transition depending on the various parameters in the system. For (64) the transition is hard for $q_0=q\sin\gamma>0$ and soft for $q_0<0$.

Figure 20 summarizes our results on the effect of asymmetry for this case. In the soft case, $q_0<0$, we state results for the attractor width Δ in the various regimes. Note the close qualitative similarity of the $q>0$ region with Fig. 6 for the case of symmetric coupling.

As before, the results for the scaling of τ are obtained from (20). The scalings for $\overline{n}$, however, are now modified, and are obtained from the differential equation approximation to (64) near $x=0$,

$$\frac{dy}{dn}=\epsilon y+y^2+q_0. \tag{65}$$

From this we obtain

$$\overline{n}\approx\int_0^{\Delta}\frac{dy}{q_0+\epsilon y+y^2}. \tag{66}$$

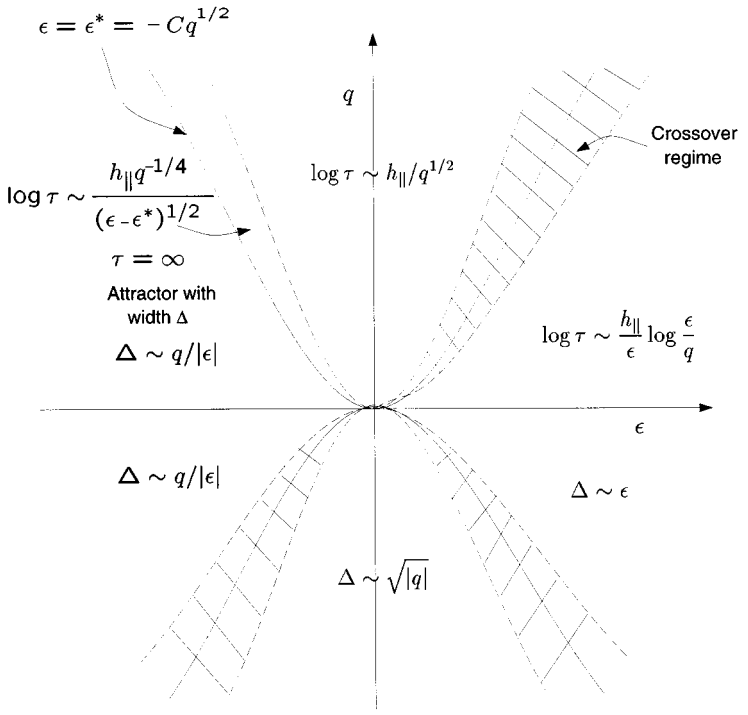

FIG. 20. A schematic representation of the results for the model with asymmetric coupling. The scalings in the various regions of the parameter space are shown.

Approximating this integral in the relevant parameter ranges and using (20), we obtain the results for τ in Fig. 20. To obtain the results for Δ, we note that the furthest extent of the attractor (when the attractor is limited to the region near $y=0$) is determined by an $x=0$ fixed point on the outer edge of the attractor. Setting $x=0$ and $y_n=y_{n+1}$ in (64), we obtain ($\Delta=|y_n|$)

$$\Delta=\left|\frac{-\epsilon\pm\sqrt{\epsilon^2-4q_0}}{2}\right|, \tag{67}$$

with the appropriate choice of the plus or minus sign, which yields the results for Δ in Fig. 20. The crisis at $\epsilon=\epsilon^*(q)$, occurs when two fixed points at $x=0$ merge. Therefore, $[\epsilon^*(q)]^2=4q_0$, i.e.,

$$\epsilon^*(q)\sim q^{1/2}. \tag{68}$$

IX. CONCLUSIONS

In this paper we study the effects of a small asymmetry and additive noise on systems that would have an invariant manifold if there was no asymmetry or noise. The invariant manifold is destroyed if we have a small asymmetry or additive noise. We derive scaling relations for the average length of the chaotic transient τ, the attractor width, and the bifurcation parameters at crisis, and we numerically verify the predicted scalings.

In physical experiments, unavoidable small asymmetry and noise limit the observability of riddled basins and induce intermittent bursting. Our results delineate the time scale over which the noiseless symmetric idealization is relevant in experiments near the bubbling transition.

ACKNOWLEDGEMENTS

This research was supported by the Office of Naval Research, by the U.S. Department of Energy (Offices of Scientific Computing and Energy Research), and by the National Science Foundation (Divisions of Mathematical and Physical Sciences). The numerical computations reported in this paper were made possible by a grant from the W. M. Keck foundation.

[1] P. Ashwin, J. Buescu, and I. N. Stewart, Phys. Lett. A **193**, 126 (1994).
[2] P. Ashwin, J. Buescu, and I. N. Stewart, Nonlinearity, **9**, 703 (1996).
[3] N. Platt, E. A. Spiegel, and C. Tresser, Phys. Rev. Lett. **70**, 279 (1993).
[4] N. Platt, S. M. Hammel, and J. F. Heagy, Phys. Rev. Lett. **72**, 3498 (1994).
[5] E. Ott and J. C. Sommerer, Phys. Lett. A **188**, 39 (1994).
[6] J. C. Alexander, J. A. Yorke, Z. You, and I. Kan, Int. J. Bifurc. Chaos **2**, 795 (1992); E. Ott, J. C. Sommerer, J. C. Alexander, I. Kan, and J. A. Yorke, Phys. Rev. Lett. **71**, 4134 (1993); J. C. Sommerer and E. Ott, Nature **365**, 136 (1993).
[7] E. Ott, J. C. Alexander, I. Kan, J. C. Sommerer, and J. A. Yorke, Physica D **76**, 384 (1994).
[8] In the above and in the rest of the paper we assume that ϵ is always close to the critical bubbling value ϵ_b. Thus $\epsilon<\epsilon_b$ ($\epsilon>\epsilon_b$) means that ϵ is less (greater) than ϵ_b, but *close* to ϵ_b. We note that for ϵ far from ϵ_b other bifurcations are also possible, most notably there can be a *blowout bifurcation* [5] at

a critical value $\epsilon=\epsilon_c>\epsilon_b$. As ϵ is increased from ϵ_b to ϵ_c more and more periodic orbits embedded in A become transversely unstable until as ϵ is increased through ϵ_c, the set A becomes unstable *on average*, i.e., the Lyapunov exponent for transverse perturbations becomes positive. (Note that the Lyapunov exponents for a chaotic attractor are expressible as averages of the Lyapunov exponents of the unstable periodic orbits embedded in the attractor.) The phenomena associated with the blowout bifurcation have received much recent attention [3–7]. In particular, if there is a riddled basin for $\epsilon_b<\epsilon<\epsilon_c$, it is destroyed as ϵ is increased through ϵ_c. If there is no riddled basin for $\epsilon_b<\epsilon<\epsilon_c$, then as ϵ is increased through ϵ_c, an extreme form of intermittent bursting called *on-off intermittency* [3] takes place. See Refs. [2–5,9] for further discussion of these phenomena.

[9] S. C. Venkataramani, T. M. Antonsen, E. Ott, and J. C. Sommerer, Phys. Lett. A **207**, 173 (1995); Physica D (to be published); A. Čenys, A. Namajūnas, A. Tamaševičius, and T. Schneider, Phys. Lett. A **213**, 259 (1996).

[10] The recent paper Ref. [18] considered the effect of asymmetry on the bubbling transition as a function of asymmetry strength precisely at the bifurcation point of the symmetric system $\epsilon=\epsilon_b$. Our treatment is more general in that it considers the behavior as a function of both asymmetry strength and ϵ, and also treats the effect of noise.

[11] J. F. Heagy, T. L. Carroll, and L. M. Pecora, Phys. Rev. Lett. **73**, 3528 (1994).

[12] D. J. Gauthier and J. C. Bienfang (unpublished).

[13] J. F. Heagy, T. L. Carroll, and L. M. Pecora, Phys. Rev. E **52**, R1253 (1995).

[14] B. R. Hunt and E. Ott, Phys. Rev. Lett. **76**, 2254 (1996).

[15] The possibility that the bubbling transition is typically triggered by a low-period periodic orbit was suggested by J. A. Yorke.

[16] We use the notation $a(x)\sim b(x)$ to denote equality to within a multiplicative factor of the quantities $a(x)$ and $b(x)$ as the parameter x is varied.

[17] C. Grebogi, E. Ott, and J. A. Yorke, Phys. Rev. Lett. **50**, 935 (1983); Ergodic Theory Dyn. Syst. **5**, 341 (1985).

[18] Y. C. Lai, C. Grebogi, J. A. Yorke, and S. C. Venkataramani (unpublished).

[19] We use the notation $a(x)\simeq b(x)$ to denote equality to within an additive constant of the quantities $a(x)$ and $b(x)$ as the parameter x is varied.